AD-A069 570 ADMIRALTY MARINE TECHNOLOGY ESTABLISHMENT TEDDINGTON--ETC F/G 20/4
ASSESSMENT OF A METHOD FOR PREDICTING THE DRAG AND BOUNDARY-LAY--ETC(U)
JAN 79 D J ATKINS

UNCLASSIFIED AMTE(N)/R78111 DRIC-BR-67646 NL

1 OF 1
AD
A069570

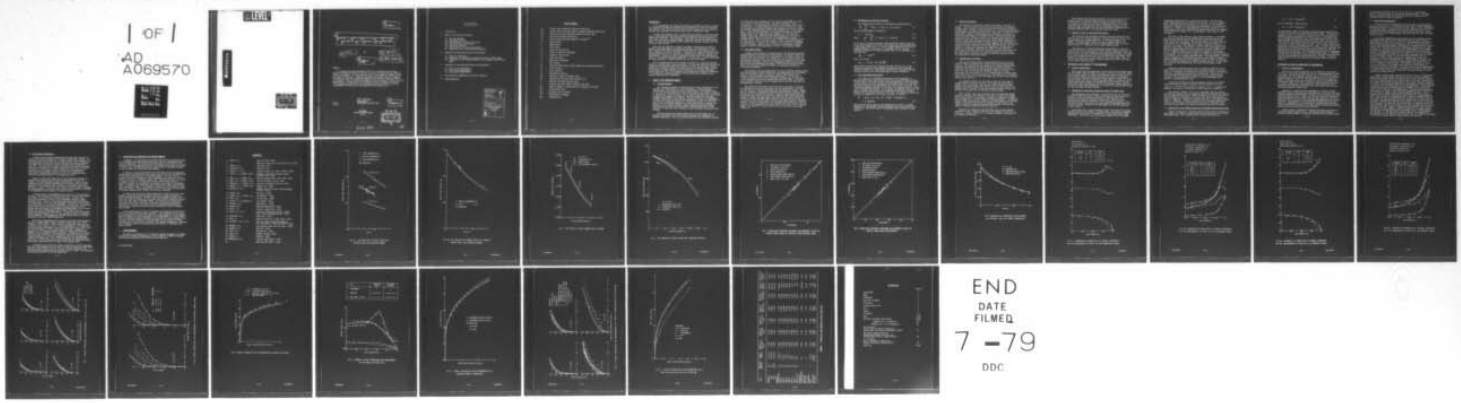

END
DATE
FILMED
7 -79
DDC

(14) AMTE(N)R78111

(6) ASSESSMENT OF A METHOD FOR PREDICTING THE DRAG AND BOUNDARY-LAYER DEVELOPMENT ON A BODY OF REVOLUTION AT ZERO INCIDENCE (U)

(12) 35 p. BY (18) DRIC

(10) D J ATKINS (19) BR-67646

Summary

A comparison between experimental data and a boundary-layer and drag prediction method for bodies of revolution at zero incidence and high Reynolds number is discussed. The only physical input to the prediction method is that of transition position. In general drag predictions agree well with measurements both in trend and in absolute magnitude and predicted velocity profiles on afterbodies with an included semi-angle of less than about 15° agree well with measurements. A modification to the method has been developed which gives a better agreement between predicted and measured velocity profiles on fuller afterbodies provided that no flow separation takes place. (U)

AMTE (Teddington)
Queens Road
TEDDINGTON Middx TW11 OLN

(11) January 1979

40 pp
18 figs

CONTENTS

LIST OF SYMBOLS

C_A	Profile drag coefficient based on wetted area.
C_D	Profile drag coefficient based on maximum cross-sectional area.
C_F	Skin-friction drag coefficient based on wetted area.
C_f	Local skin-friction coefficient.
C_V	Profile drag coefficient based on $(\text{volume})^{2/3}$.
D	Body diameter.
H	Shape factor.
L	Body length.
L_n	Length of nose section.
L_c	Length of parallel centrebody.
L_t	Length of tail section.
n	Power-law index.
P	Wake defect parameter.
r	Body radius.
R_L	Reynolds number based on body length and free-stream velocity.
U	Local velocity.
U_t	Total velocity.
U_o	Free-stream velocity.
U_1	Velocity at edge of boundary layer.
$\bar{U}_1$	Hypothetical velocity used in section 2.4.
x	Distance from nose along the axis.
y	Distance from hull along a normal to the hull.
α	Angle of tangent to body surface with respect to the axis.
Δ^*	Displacement area.
δ	Boundary layer thickness.
δ^*	Displacement thickness.
θ	Momentum area.

INTRODUCTION

In the development and feasibility studies of underwater vehicles, methods for predicting the drag and boundary layer development of a body of revolution are required. They can be used to provide initial estimates of drag, possibly reducing the requirement for costly wind-tunnel or towing-tank tests.

A widely used boundary layer and drag prediction method in the UK has been that of Young [1] which was used to produce the Engineering Sciences Data Unit (ESDU) data items [2] . The accuracy of this method is limited inasmuch as it only takes into account Reynolds number, transition position and body fineness ratio. It does not distinguish between bodies with the same fineness ratio but different body contours.

There are now available a number of methods for predicting the drag and boundary layer development of axisymmetric bodies. The method used in this Report was obtained from Dr Myring of Salford University and details of how to use it appear in an earlier Note [3] . In Reference 3, predicted boundary layer integral parameters on the afterbody are compared with estimates obtained from measurements. In general, there is agreement between theory and experiment in trend, if not always in absolute magnitude. In particular, on blunt afterbodies, the shape parameter is under-predicted near the tip of the body.

One of the applications of the prediction method is to determine scaling effects on boundary layer velocity profiles. In this case values of the velocity components are required rather than integrals of them. In the present Report, predicted and measured velocity profiles on slender afterbodies agree well but the agreement is less favourable on afterbodies with an included semi-angle greater than about 15°. This disparity is discussed and a method of overcoming it is examined by comparing predicted velocity profiles and boundary layer integral parameters with experiment.

2. THEORY OF THE PREDICTION METHOD

2.1 Previous methods.

All theoretical methods of drag prediction involve calculation of the boundary layer development over the body surface. Young [1] showed theoretically that the profile drag is proportional to the momentum area of the wake far downstream of the tail and he related the values at infinity to those at the tip of the body. In the turbulent boundary layer calculation an experimental pressure distribution was used as input and the shape parameter was assumed to be constant. Granville [4] used a one-parameter integral method which allowed the shape parameter to vary and incorporated a criterion for predicting transition. More recently Cebici et al [5, 6] used a finite difference method with a simple eddy viscosity approach for modelling the Reynolds stresses. Hess & James [7] using this method demonstrated that great care was needed in extrapolating from an axial station at or near the tip to infinity in order to obtain the correct value of drag.

Previous calculation methods suffer from the disadvantage that the pressure distribution over the body surface needs to be calculated or measured separately. There are accurate potential flow calculation methods

for doing this even on sharply curved or pointed bodies [8], but these do not take the wake into account. The usual technique in this circumstance is to extrapolate the potential flow pressure distribution into the wake. A further drawback at the tail end of the body is that the boundary layer thickness becomes large compared with the body radius and the usual assumptions associated with boundary layer theory cease to apply. Also on full afterbodies, the pressure distribution predicted using potential flow theory does not correspond to that which the boundary layer sees. Nakayama & Patel [9] overcame this by using an integral method adapted to calculate thick axisymmetric turbulent boundary layers. After each step in the boundary layer calculation over the last ten per cent of the body length, a value of drag was computed by extrapolation to infinity and the final value chosen was the maximum of those obtained. Kerney & White [10] used a two-parameter integral method of Granville [11] applicable to thick or thin boundary layers.

2.2 The present method.

A method which attempts to overcome most of the previously mentioned disadvantages has been developed by Myring [12]. The method couples the boundary layer and potential flow calculations in an iterative cycle and the potential flow calculation is carried out over the body surface plus displacement thickness. The entire calculation is extended into the wake where at some prescribed location the displacement surface is truncated and suitable end conditions are imposed. Apart from the details of body shape the only inputs required are those of transition position and free-stream conditions.

The potential flow calculations uses the well established surface source distribution method of Hess & Smith [8]. The laminar part of the boundary layer is calculated using the method of Luxton & Young [13] and the turbulent part using Head's entrainment method [14]. The far wake is treated by using an alternative entrainment hypothesis and the near wake by interpolation between the attached flow and the far wake. The profile drag is computed from the value of momentum area in the far wake which is extrapolated to infinity.

The method also calculates the skin-friction drag which is obtained by integrating the local skin-friction over the body surface. Two skin-friction laws are currently programmed into the prediction method. Myring used the empirical relationship of Ludwieg & Tillman [15]. Chappell [16] pointed out that for Reynolds numbers R_L (based on body length) above 10^7 the skin-friction drag of a flat plate predicted using this relationship begins to diverge from experimental data, and that for slender bodies of revolution at high Reynolds number ($R_L > 10^8$) the predicted total body drag is less than that of a flat plate with the same surface area and transition position. Chappell [17] modified the Ludwieg-Tillman expression to provide a better fit to experimental flat plate data over a wider range of Reynolds number. The modified law agrees well with flat plate data in the range $10^5 < R_L < 10^9$.

2.3 Determination of velocity profiles.

The method predicts directly, the momentum area θ defined by

$$\theta = \int_0^{\delta} (U/U_1)\,(1 - U/U_1)\,(r + y\cos\alpha)\,dy \qquad (1)$$

and the shape parameter H defined by

$$H = \Delta^*/\theta \qquad (2)$$

where

$$\Delta^* = \int_0^{\delta} (1 - U/U_1)\,(r + y\cos\alpha)\,dy \qquad (3)$$

In (1) and (3) r denotes the body radius and α the angle of the body surface with respect to the axis. The integrations are performed along a line normal to the hull. In order to obtain values of the velocity component parallel to the hull, it is assumed that the velocity distribution across the attached boundary layer can be expressed in a power-law form

$$U/U_1 = (y/\delta)^{1/n} \qquad (4)$$

while in the wake

$$U/U_1 = 1-P\left\{1 + \cos(\pi y/\delta)\right\} \qquad (5)$$

where (1-2P) is the value of U/U_1 on the wake centre line. In the calculation procedure, the parameters δ (boundary layer thickness), n (power-law index) and P (wake defect parameter) are estimated from the external conditions and the boundary-layer integral parameters.

2.4 Full after-body modification.

As a result of a preliminary assessment of the method [3], a modification has been developed for full after-bodies following the work of Patel [18]. Patel used a method requiring knowledge of the longitudinal pressure gradient both at the edge of the boundary layer and at the wall, and showed using hot wire measurements that they were not the same. The longitudinal pressure gradient at the edge of the boundary layer is related to the corresponding velocity. Let U_1 denote the measured velocity at the edge of boundary layer and $\bar{U}_1$ the corresponding hypothetical velocity deduced from the pressure gradient at the wall. The prediction method was modified by assuming that U_1 and $\bar{U}_1$ are related as follows:

$$\bar{U}_1 = U_1\left\{1 - (15 - |x - L|)/225\right\} \quad (0.85<x/L<1.15)$$

$$= U_1 \text{ elsewhere} \qquad (6)$$

This empirical law is based on the measurements of Patel et al [19]. Suppose U_1 is the external velocity predicted using the potential flow calculation. The $\bar{U}_1$ was used in the boundary layer computation rather than U_1.

2.5 Transition position.

The location of the natural transition position is difficult to predict. Several different criteria have been proposed for bodies of revolution and a review of these was carried out by Granville [20] and by Kaups [21]. According to both authors none of the available prediction methods agrees well with experiment over a wide range of conditions and body shapes. Granville however deduced an empirical correlation of transition measurements on streamline bodies. Nakayama and Patel [9] incorporated four different criteria in a boundary layer prediction method and these gave results which often agreed among themselves, but differed widely from the observed values. The available experimental evidence (surveyed by McCarthy et al [22]) suggests that the position of natural transition varies with nose shape, Reynolds number, the level of turbulence in the free-stream and the roughness of the body surface. However, in practice, at high Reynolds number and high prismatic coefficient ($4V/\pi D^2L$), transition is likely to occur well forward and will normally be controlled by a tripping mechanism in model tests. For these reasons transition position is prescribed explicitly rather than predicted in the present method.

2.6 Limitations of the method.

There are situations where the prediction method will not work owing to numerical instabilities arising though the viscous-inviscid coupling. The instabilities are caused by the laminar boundary layer method becoming unstable in large favourable or adverse pressure gradients. The most significant practical example of this is a body with a flat nose, often used for torpedoes. One way to obtain predictions for such a body is to fit a hemispherical or elliptic nose, which gives rise to added uncertainties in the accuracy of the results, which are not large if the flat nose shape does not give rise to laminar separation on the nose.

An assumption inherent in the method is that the flow does not separate before the tip of the body. This means that very blunt or rounded tails are excluded. Experimental evidence mentioned below suggests that laminar separation from the nose will only occur at low Reynolds numbers (typical of wind tunnel models) which can usually be avoided by the proper use of turbulence stimulation [22].

Some instances have been encountered where the prediction method failed to converge. For example, in the case of a body with a hemispherical nose followed by a length of parallel centrebody, the method only converged over a limited range of transition position. In practice, laminar separation was known to exist on this body shape at low Reynolds numbers. The method also failed to converge for some bodies with a length of parallel centrebody greater than about half the total body length at Reynolds numbers R_L less than about 10^7.

Normally the computations were performed with a drag iteration tolerance of 0.001. However, this had to be increased to 0.003 for a body with a fineness ratio $L/D = 4$ at Reynolds number R_L less than 10^7 for reasons of stability.

The prediction method has been modified to allow for the effect of a simple, lightly-loaded propulsor and this will be described in a future report. In practice, control surfaces are also fitted to the tail region which make the flow highly three-dimensional. The effect of these cannot be incorporated into an axisymmetric method, but the additional drag resulting from these and from surface roughness can be estimated [23] and added to the bare-hull predicted value.

2.7 Sources of error in the prediction method.

This topic has been discussed by Myring [12], who showed that any error in the level of skin friction is likely to lead to an error in the drag estimation of the same magnitude. In addition because of the assumed relationship between skin friction and shape parameter, as defined in reference [12], a 1% error in shape parameter over the entire body can lead to a 1.6% error in the value of profile drag.

Unfortunately, accurate boundary-layer measurements on a body of revolution are scarce. Probably the most detailed results available are those of Patel et al [19] obtained using a hot-wire anemometer. Over the latter half of the body, predictions and measurements of shape factor [3] are in good agreement except over the last 10% of the body length. This disparity will have only a small effect on the profile drag. Hence any error in the prediction of profile drag is likely to be due to an error in the level of skin-friction.

3. COMPARISON OF DRAG PREDICTIONS WITH EXPERIMENT

3.1 Myring's comparisons.

Myring [12] has made comparisons of drag predictions and measurements for the airship 'Akron' [24] and two bodies, A and B, of Lyon [25]. Three different-sized models of 'Akron' gave different values of drag, those of the two larger models being 7% and 14% less than that of the smallest. Both Young's and Myring's methods gave almost identical results which are slightly larger than that for the medium sized model. For Lyon's A and B, Young's method gave somewhat better agreement with experiment, Myring's predictions being about 8% less than the measurements. Myring pointed out however that Lyon's measurements may be in error by as much as 10% because of tunnel blockage and other effects.

3.2 Comparison of predicted and measured values of profile drag.

The experimental data discussed in this section were all obtained in a situation where there was no laminar separation and where either the location of natural transition was known or transition was fixed artificially by means of turbulence stimulation. Predictions were obtained with transition specified at the corresponding location. All the predictions in this section were made using the Ludwieg-Tillman skin-friction law [15]. Details of the body shapes and flow conditions are listed in Table 1.

Predictions over a range of Reynolds number were obtained for three streamline bodies with different fineness ratios, referred to as DTMB4154, 4159 and 4165, and tested in a towing tank at David Taylor Model Basin (DTMB) [26]. The drag of body 4165 was also measured by ARL (now AMTE

(Teddington)) [27] mainly in low speed wind tunnels, from both drag balance measurements and pitot-static wake surveys. In all the measurements, transition was fixed by means of a trip wire or other similar mechanism. Comparison of predictions and measurements is illustrated as Figure 1(a). Balance and wake measurements were also carried out on a torpedo-shaped body with a hemispherical nose [27] and these are compared with predictions in Figure 1(b). The agreement in both cases is very favourable.

The effect of nose shape on drag is shown in Figure 2. Nose shape was varied by changing the nose fineness ratio while keeping the nose shape constant and the total volume was kept constant by varying the length of parallel centrebody. The profile drag of the bodies, referred to as 4620-1 to 4, was measured over a range of Reynolds number by McCarthy et al [22]. The location of natural transition was determined using hot film probes. Transition on the two fullest nose shapes was a result of laminar separation which occurred at the same location at all the test Reynolds numbers, but the separation bubbles so formed were short in length and the parasitic drag due to separation was assumed to be negligible. On the other two bodies, the position of natural transition moved forward with increasing Reynolds number. The measurements of profile drag are compared with predictions using the present method, and with predictions [22] using the finite difference method of Cebici & Smith [7]. The two theoretical methods give almost identical results. In both cases the trends are well predicted but the actual values slightly underpredicted.

Comparisons illustrating the effect of transition position on the drag of Lyon's bodies A and B [25] (both streamline shapes) is shown in Figure 3. Transition was controlled by varying the level in the oncoming flow using the presence or absence of a wire screen. The trends are correctly predicted although the absolute values are slightly underpredicted. As mentioned above (section 3.1) the measurements may be subject to some experimental error.

Correlations between predicted and measured values of the profile drag coefficients C_D (based on maximum cross sectional area) and C_V (based on (volume)$^{2/3}$) are presented in Figures 4 and 5. In general the agreement is as good as the accuracy to which drag can be measured.

The results in Figures 4 and 5 are in agreement with some results presented by Chappell [16], who compared predictions using Myring's method with the ESDU data sheets [2]. These data sheets give C_D as a function of Reynolds number and fineness ratio L/D and they were derived using the method of Young [1]. Chappell's conclusion was that in the Reynolds number range $2 \times 10^6 < R_L < 2 \times 10^7$ Myring's method with the Ludwieg-Tillman skin-friction law is likely to give values of drag correct to about $\pm$ 5%, a reduction of about 50% on the likely errors using the ESDU data sheets.

3.3 Comparison of the Ludwieg-Tillman and the Chappell skin-friction laws.

Figure 6 illustrates a comparison between predictions of skin-friction drag coefficient (based on wetted area) and two correlations of flat plate experimental data. The correlations are the ITTC line given by

$$C_F = 0.075 / (\log_{10} R_L - 2)^2 \qquad (7)$$

and the Schoenherr formula given by

$$C_F = 0.242 / \log_{10}(R_L C_F)^2 \qquad (8)$$

At low Reynolds numbers the Schoenherr formula deviates slightly from the ITTC line and this is discussed by Granville [28]. The predictions in Figure 6 are for a body with a fineness ratio (L/D) of ten-to-one (DTMB 4159) [26], using Myring's method with both the Ludwieg-Tillman and the Chappell skin-friction laws. Some computations with both laws were also made on bodies with fineness ratios of seven- and four-to-one (DTMB 4157 and 4154 respectively) and the results for the former body were close to those of the ten-to-one body. In all cases transition was prescribed to occur well-forward (at $x/L = 0.05$). On simple theoretical grounds one would expect the results with increasing L/D to approach from above those of a flat plate and these trends are observed using the Chappell skin-friction law. With the Ludwieg-Tillman law the corresponding values are 10-15% lower in the Reynolds number range $4 \times 10^8 < R_L < 10^9$. In some cases the predicted values of profile drag coefficient were less than the corresponding flat plate skin-friction values. At Reynolds numbers below 2×10^7 both skin-friction laws gave almost identical results.

4. COMPARISONS OF VELOCITY PREDICTIONS AND MEASUREMENTS

4.1 Patel et al measurements.

This section contains comparison of the unmodified and modified (section 2.4) prediction methods with the hot wire measurements of Patel et al. [19] The test body had a conical tail of about 23° semi-angle, nevertheless the flow remained attached right up to the tip at the test Reynolds number of 1.26×10^6. The variation of velocity components across the boundary layer were obtained at a number of different axial stations and these can be used to obtain integral parameters which can be directly compared with the predictions. Values of skin-friction coefficient were measured using three different methods and there was reasonable agreement between them.

Comparison of predictions and measurements of various integral parameters using the Myring prediction method with and without the blunt after-body modification mentioned in section 2.4 and equation 6 are presented as Figures 7 and 8. Figures 7(a) and 7(b) taken from reference 3, using the unmodified theory, show that the shape parameter H is underpredicted near the tip of the body although the momentum area θ is well predicted. Incorporation of the modification (Figures 8(a) and 8(b)) leads to an improvement in the prediction of shape parameter and skin-friction coefficient although the external velocity distribution and the momentum area are slightly less well predicted.

Figure 9 shows a comparison of measured and predicted profiles of velocity component along the hull. The improved shape parameter prediction clearly leads to an improved prediction of the general shape

of the velocity profiles near the tip of the body. In particular, values of velocity close to the hull are better predicted. The agreement is good considering the limitations imposed by assuming a one-parameter family of velocity profiles.

4.2 Water-tunnel measurements.

A number of velocity measurements have been made on torpedo-shaped bodies of revolution in the thirty-inch water tunnel at AMTE (Teddington). The bodies referred to in this section all had conical tails of semi-angle 16° and flat noses. Hemispherical or elliptic noses were used in the boundary-layer calculations to obtain the velocity predictions. However the effect of this on boundary-layer predictions near the tip of the body should be small.

Some velocity measurements were carried out on an unpowered torpedo model using three rakes of total head tubes with the static pressure determined from static holes in the hull. The measurements were made in planes normal to the hull corresponding to those of the predictions at two different Reynolds numbers. Comparison of the measured total velocity profiles with the predicted velocity components along the hull is shown in Figure 10. There is some scatter on the measurements and the agreement between measurements and predictions deteriorates with downstream position. One possible reason for this disparity is the error introduced in the measurements by assuming that the static pressure does not change across the boundary layer. As one moves downstream there may be a variation in static pressure across the boundary layer which would introduce an error in the measurements. Another possible reason is that measurements of total velocity are being compared with predictions of velocity component along the hull. The greatest discrepancy is likely to be at the edge of the boundary layer where the flow is axial, in which case the predictions ought to be about 4% less than the measurements. At the most downstream position the disparity is in excess of 10% across the whole boundary layer, which means that the latter correction is not sufficient to account for it.

A single boundary layer traverse was carried out on a torpedo-shaped body similar to the previous one, but fitted with a fin-duct assembly. Velocity was measured using a pitotstatic tube a short distance upstream of the duct leading edge and in a plane normal to the axis. Predictions in this plane were obtained by assuming that the velocity component parallel to the hull does not change along a line drawn parallel to the hull between the plane of the predictions and that of the measurements. From Figure 11 in which predictions and measurements are compared, it is evident that there is little scatter on the measurements. The predictions labelled as 'uncorrected' in Figure 11 agree with the measurements near to the hull, but they deviate slightly with increasing distance from hull. This disparity can be largely explained by considering that the measurements are of total velocity and predictions are of velocity component along the hull. Near the hull the streamlines will be parallel to the hull but at the edge of the boundary layer the total velocity will be almost axial in direction. Between these extremes the direction of flow will vary between the two values. To obtain the total head value, the component along the hull should be divided by the cosine of the angle between the flow and the hull and vice versa. Figure 11 shows predicted values of total velocity calculated this way, assuming a uniform variation of flow angle between the hull and the predicted edge of the boundary layer. The agreement is now improved. At the edge of the boundary layer, a flow angle of 16°, the correction to the predicted value is about 4%. At a corresponding angle of 12° the correction would be about 2% and at 20° about 6%.

4.3 Wind-tunnel measurements.

A number of wind tunnel measurements have been made on bodies of revolution by AMTE (Teddington) in the NMI low-speed wind tunnels. Two different bodies were tested, one a streamline body with a maximum tailcone semi-angle of about 13° and the other having a length of parallel centrebody with a much fuller conical after-end with a semi-angle of about 22°. The hull static pressure distribution was measured and wake surveys were conducted at one axial station near the tip on the former body and two on the latter, using a pitotstatic probe connected to traversing gear programmed to move in radial and circumferential directions. These surveys showed the flow to be axisymmetric apart from the region downstream of a thin supporting strut.

Figure 12 (taken from reference 3) shows comparisons between the measured and predicted external velocity distributions, which are related to the corresponding pressure distributions. Figure 13 shows comparison between velocity measurements and predictions at one axial position on the streamline body, corrected in the manner described in section 4.2 so as to be of the total velocity along a radius. Although the shape parameter is slightly under predicted as mentioned in reference 3, the agreement between values of velocity is good.

A further series of measurements was carried out on the full-after-end body. Four rakes which could be either total or static head tubes were fixed to the tailcone at different stations. The two middle stations corresponded to those of the programmed pitotstatic probes mentioned above. Figure 14 illustrates comparison between predictions and measurements at all four rake positions. Predictions were obtained with and without the modification described in section 2.4. The measurements using the total and static head tubes show considerably more scatter than those using the programmed pitotstatic tubes. At the second station the latter measurements agree slightly better with the predictions obtained with modification. At the next station downstream neither prediction agrees well, but the unmodified method is in slightly better agreement. The measurements clearly indicate that the flow has separated at the most downstream position.

Some recent measurements were conducted on the body with full after-end with a lightly longer length of parallel middle body in the AMTE (Haslar) No 2 Ship Tank. A rake with twelve pitotstatic tubes was used to measure total velocity at $x/L = 0.985$ corresponding to the measuring position furthest downstream in the wind tunnel tests, but at about twice the Reynolds number. At this higher Reynolds number no separation is present, but the unmodified theory (Figure 15) gives slightly better agreement with the measured velocity profiles. Figures 14 and 15 illustrate that near the tip of a full afterbody, where the flow has either already separated or is close to separation, the power law assumption (equation 4) breaks down. Also, broadly speaking, the modified theory gives better velocity predictions near the hull and the unmodified theory gives better predictions near the edge of the boundary layer.

In practice, the tailcone of a body of revolution is often truncated. This will cause separation of the flow if it has now already occurred which may well have an effect on the flow for some distance upstream. The prediction method assumes that the tailcone ends in a point. The difference may account for some of the above disparities.

5. CONCLUSIONS AND SUGGESTIONS FOR FURTHER RESEARCH

In general, the drag prediction method of Myring with the skin-friction law of Chappell gives predictions which agree well with measurements both in trend and magnitude. The predicted trends correspond with those of other theoretical and semi-empirical methods. The method has now been used by ESDU to produce data item 78019 [29] on the profile drag of axisymmetric bodies at zero incidence for subcritical Mach numbers.

In general, velocity measurements and predictions using the unmodified Myring method agree moderately well, except near the tip of a full after-body. In this region, especially at low Reynolds numbers, the flow is often separated or close to separation and the assumption of a power law velocity profile, inherent in the method, breaks down. The modified theory of section 2.4 predicts values of velocity near the hull rather better than the unmodified theory, but the position is reversed at the edge of the boundary layer. In general, the unmodified theory gives better velocity predictions than the modified theory. It is hoped to be able to use the method to scale model test data on a fully appended body to full scale, where the difference in Reynolds numbers may be a factor of as much as a hundred.

At present the prediction method breaks down on bodies with flat noses, because the laminar flow method becomes unstable in large favourable or adverse pressure gradients. However, there is experimental evidence which shows that these are bodies with flat noses where laminar separation does not occur over some range of Reynolds number. The method could be modified to deal with a body with a flat nose by starting the laminar boundary-layer calculation at the end of the nose flat using boundary-layer parameters derived from a separate calculation using a differential laminar boundary-layer method.

In any real situation a body of revolution will normally be fitted with control and stabilizing fins and a propulsor. The Myring prediction method has been modified to include the effect of a single propeller on the boundary-layer development and this modification will be described in a future report. There are empirical methods available for estimating the drag increment due to fins and the thrust deduction of the propulsor, but the accuracy of these estimates and how they scale is subject to considerable uncertainty. Nevertheless the present prediction method should prove useful in feasibility and design studies.

6. ACKNOWLEDGEMENTS

The author is indebted to Dr D F Myring of Salford University for supplying the basic computer programme and to Mr P D Chappell of ESDU for helpful discussions and supplying the modified skin-friction law.

D J Atkins (HSO)

REFERENCES

1.	YOUNG, A.D.,	ARC R & M 1874 (1939)
2.		ESDU Data Items Aero B 02.04.00-02.04.03 (1973)
3.	ATKINS, D.J.,	ARL/G/N52 (1974)
4.	GRANVILLE, P.S.,	DTMB 849 (1953)
5.	CEBICI, T., et al	Douglas Aircraft Co., MDC J 0973-01 (1970)
6.	CEBICI, T., & SMITH, A.M.O.,	Analysis of Turbulent Boundary Layers Academic Press (1974)
7.	HESS, J.L., & JAMES, R.M.,	McDonnel Douglas Corp., MDC J 6791 (1975)
8.	HESS, J.L., & SMITH, A.M.O.,	Prog in Aeronautic Sci 8 (1967)
9.	NAKAYAMA, A., & PATEL, V.C.,	Iowa Inst of Hydraulic Res 151 (1973)
10.	KERNEY, K.P., & WHITE, N.M.,	DTNSRDC 4641 (1975)
11.	GRANVILLE, P.S.,	DTNSRDC 4525 (1975) also J Ship Res 22(3) 131-139 (1978)
12.	MYRING, D.F.,	RAE 72234 (1973)
13.	LUXTON, R.E., & YOUNG, A.D.,	ARC R&M 3233 (1962)
14.	HEAD, M.R.,	ARC R&M 3152 (1958)
15.	LUDWIEG, H., & TILLMAN, W.,	NACA TM1285 (1950)
16.	CHAPPELL, P.D.,	ESDU Memo 27 (1978)
17.	HODGES, M.D.,	ESDU Memo MDH/DAP/66 (1977)
18.	PATEL, V.C.,	Aeronaut Q 25(1)47-58 (1974)
19.	PATEL, V.C., et al	Iowa Inst of Hydraulic Res 142 (1973) also J Fluid Mech 63(2)345-367 (1974)
20.	GRANVILLE, P.S.,	NSRDC 3900 (1974)
21.	KAUPS, K.,	Douglas Aircraft Co., MDC J 6530 (1974)
22.	McCARTHY., J.H., et al	Proc 11th Sym on Naval Hydrodynamics Univ Coll London (1976) pp II-69 to II-95
23.	HOERNER, S.F.,	Fluid-dynamic Drag, publ by author (1958)
24.	FREEMAN, H.B.,	NACA 432 (1932)
25.	LYON, H.M.,	ARC R&M 1622 (1934)
26.	WHITE, N.M.,	DTNSRDC 77-0028 (1977)
27.	RITTER, H.,	ARL/G/N2 (1963)
28.	GRANVILLE, P.S.,	J Ship Res 21(1)30-39 (1977)
29.		ESDU Data Item 78019 (1978)

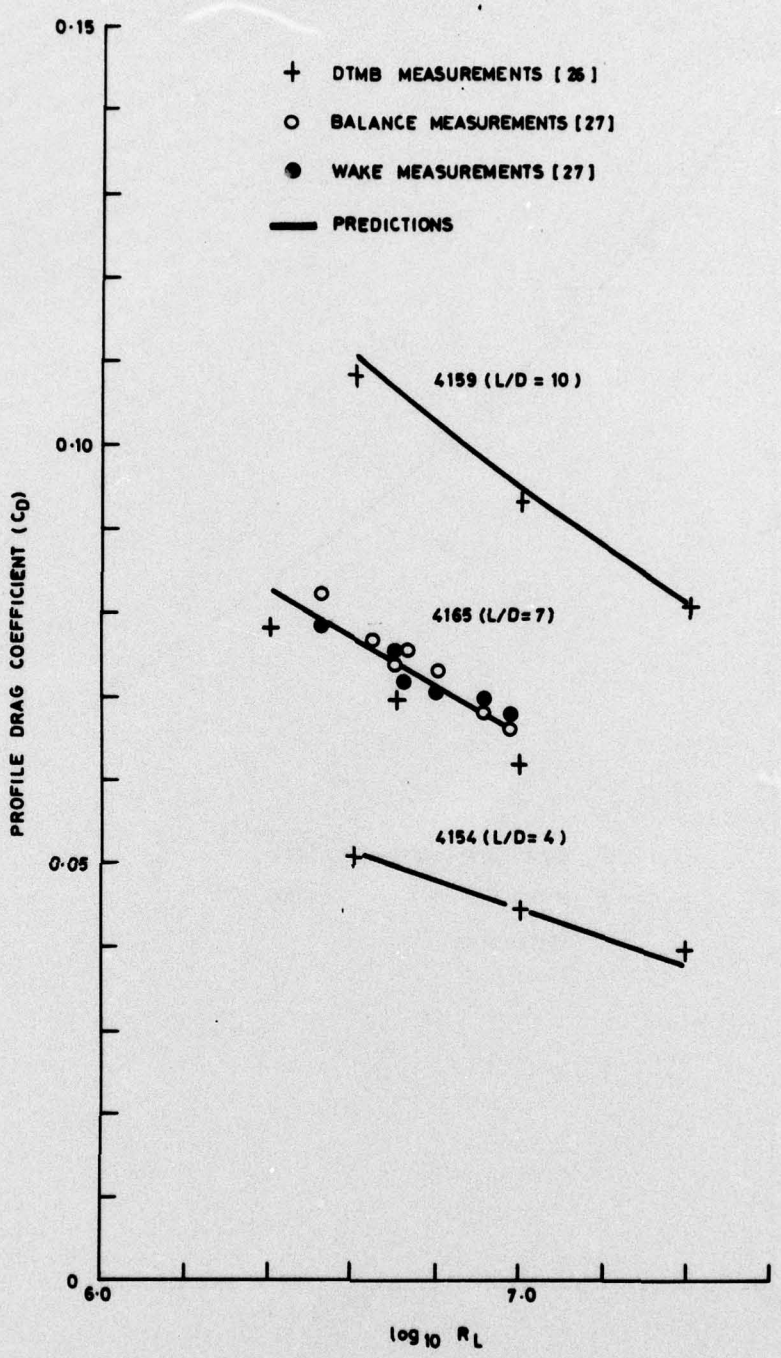

FIG. 1(a) THE VARIATION OF PROFILE DRAG WITH FINENESS RATIO AND REYNOLDS NUMBER

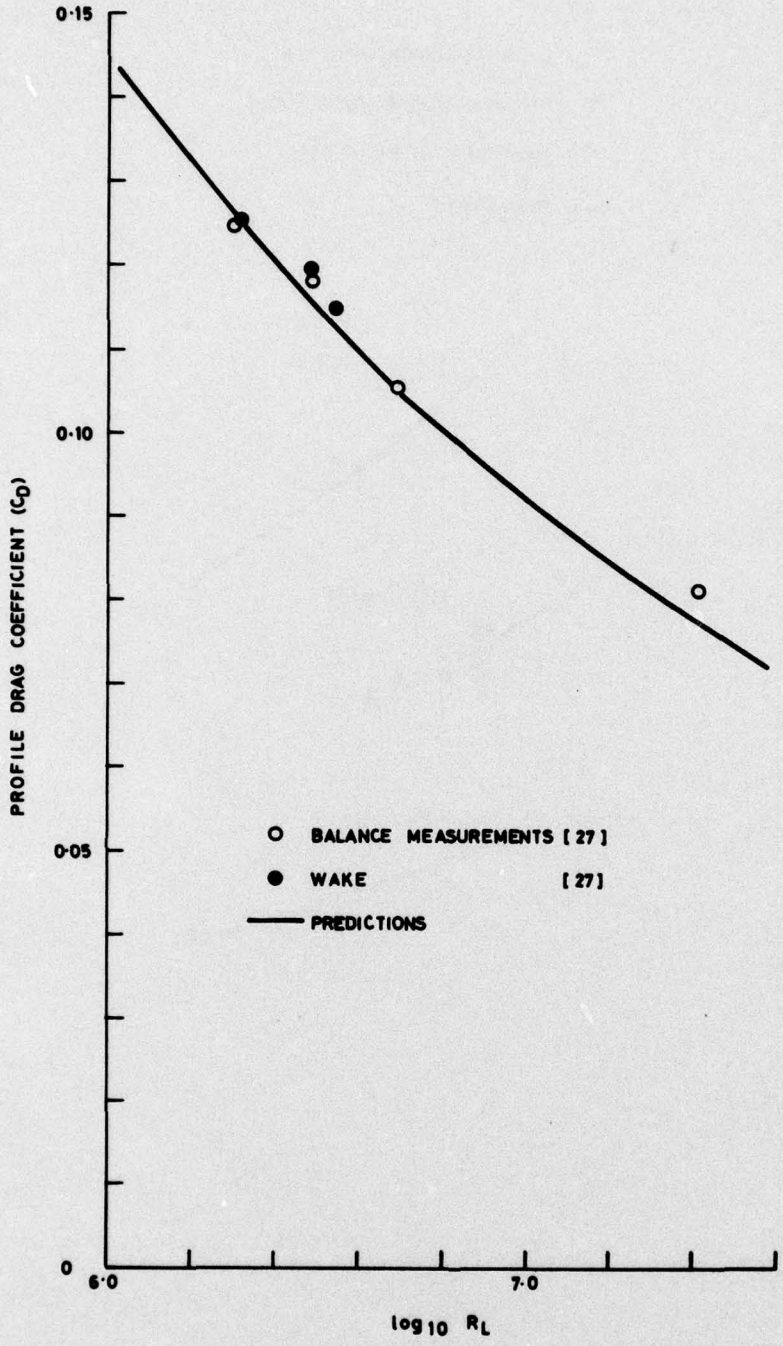

FIG. 1(b) THE VARIATION OF PROFILE DRAG OF A TORPEDO SHAPED BODY WITH REYNOLDS NUMBER

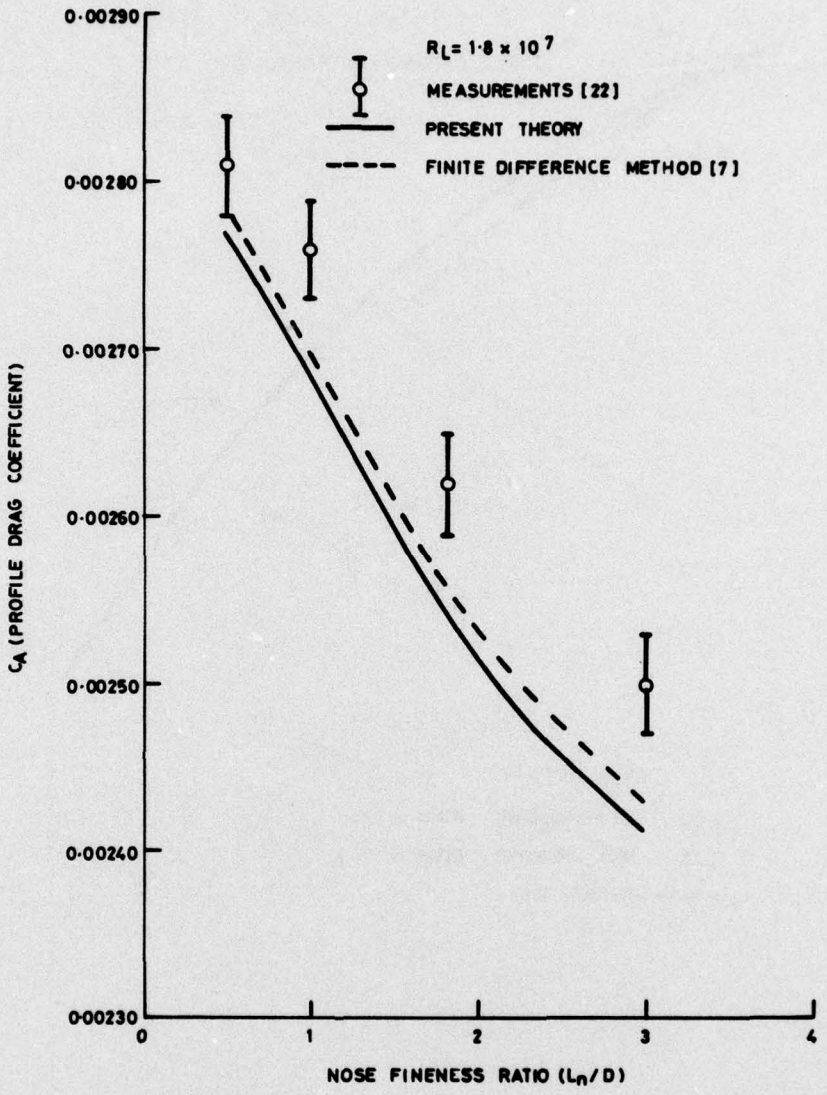

FIG. 2 THE EFFECT OF NOSE FINENESS RATIO ON DRAG

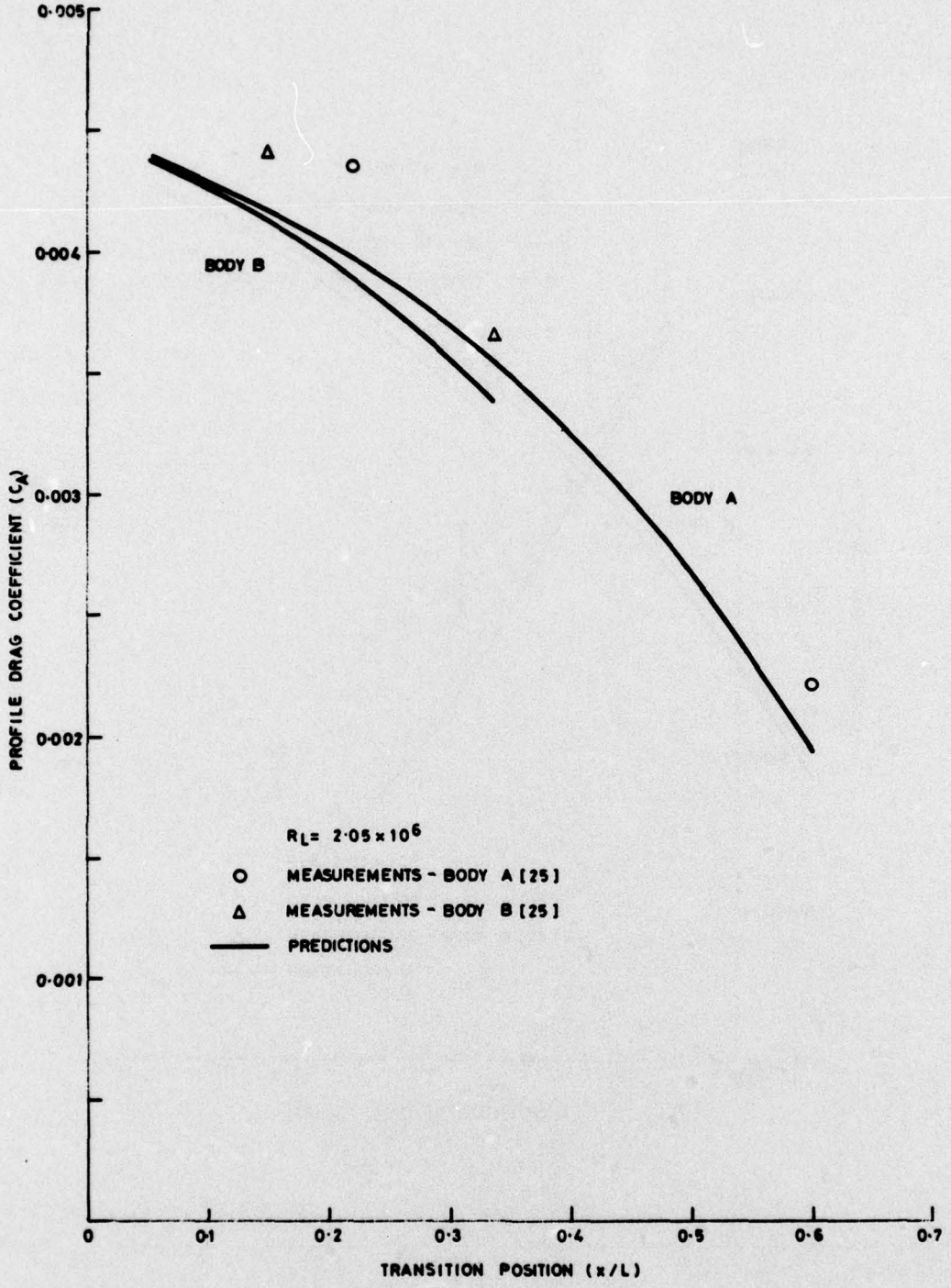

FIG. 3 THE VARIATION OF PROFILE DRAG WITH TRANSITION POSITION

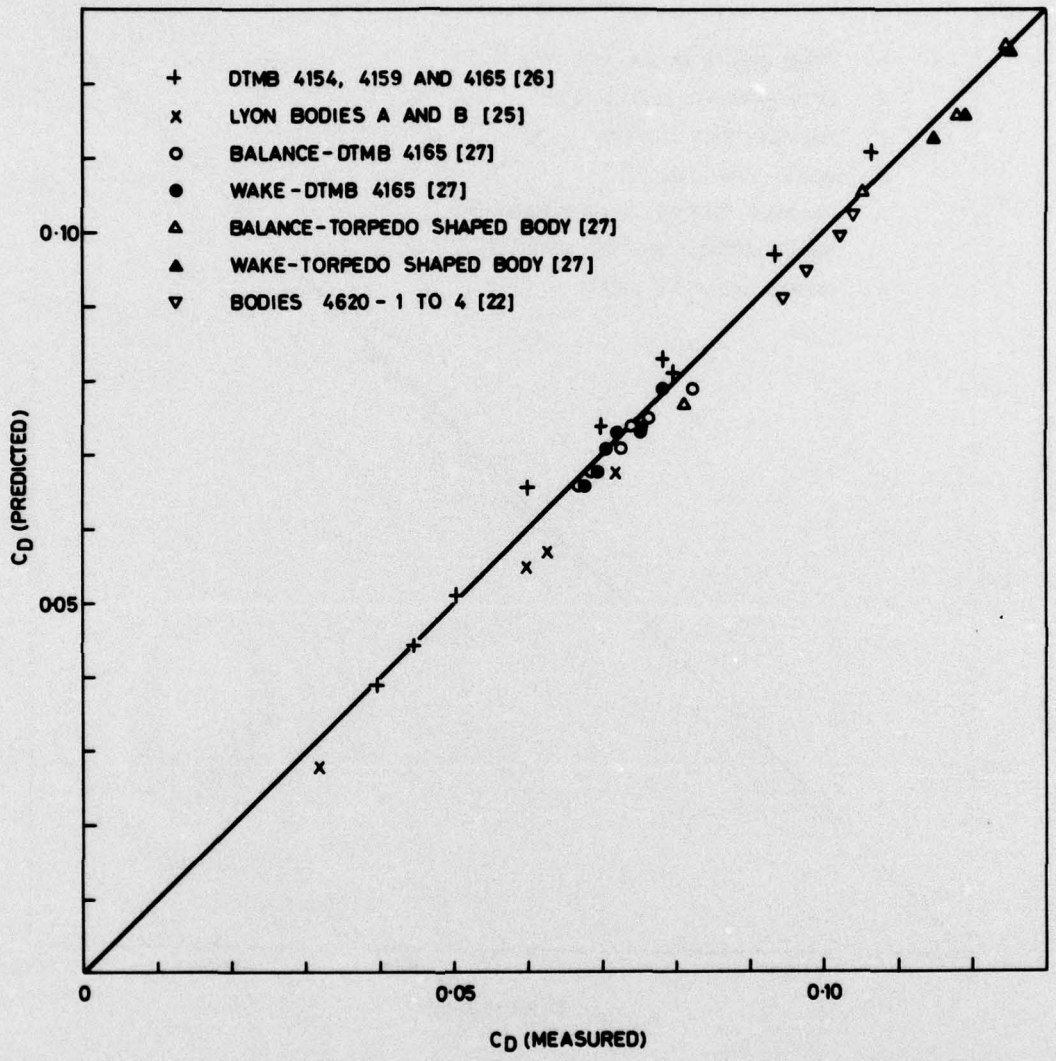

FIG. 4 CORRELATION BETWEEN MEASURED AND PREDICTED VALUES OF PROFILE DRAG BASED ON MAXIMUM CROSS-SECTIONAL AREA

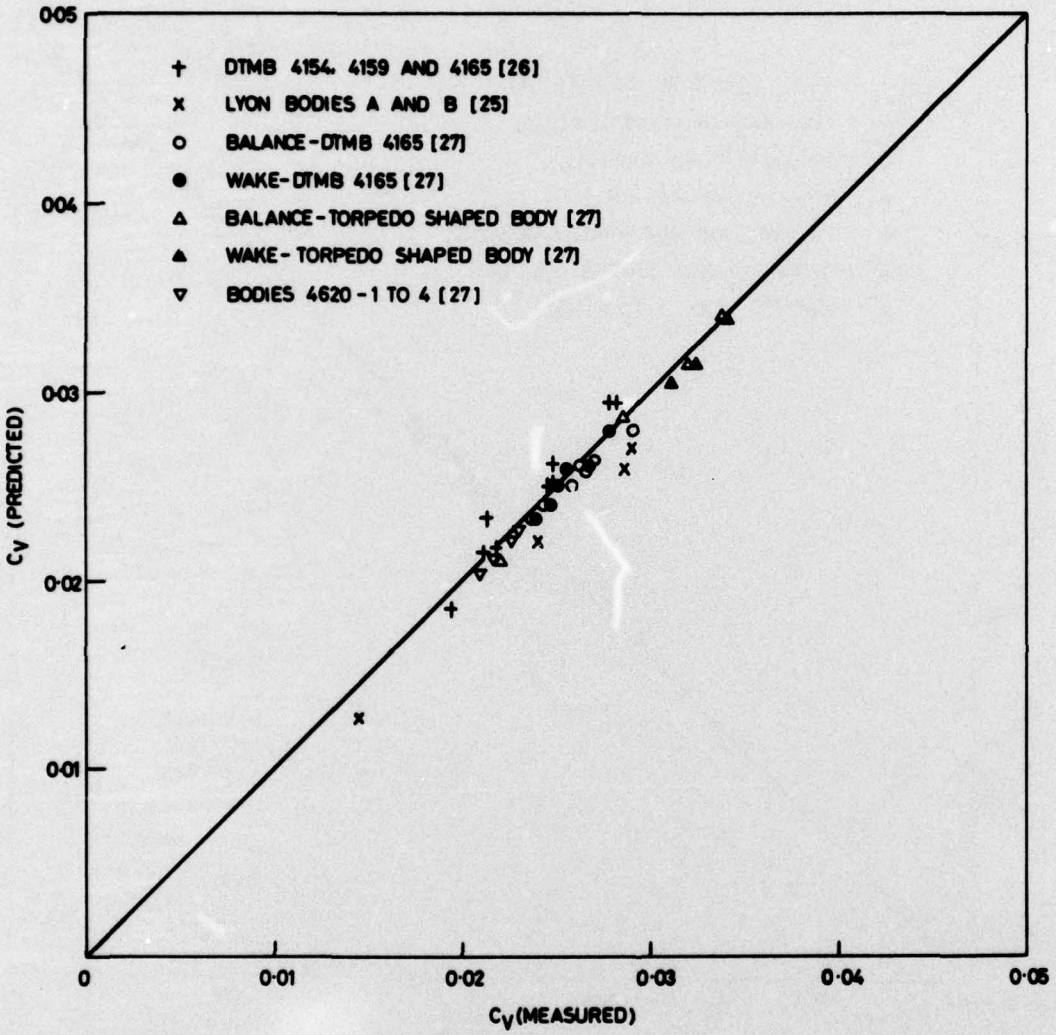

FIG. 5 CORRELATION BETWEEN MEASURED AND PREDICTED VALUES OF PROFILE DRAG BASED ON (VOLUME)$^{2/3}$

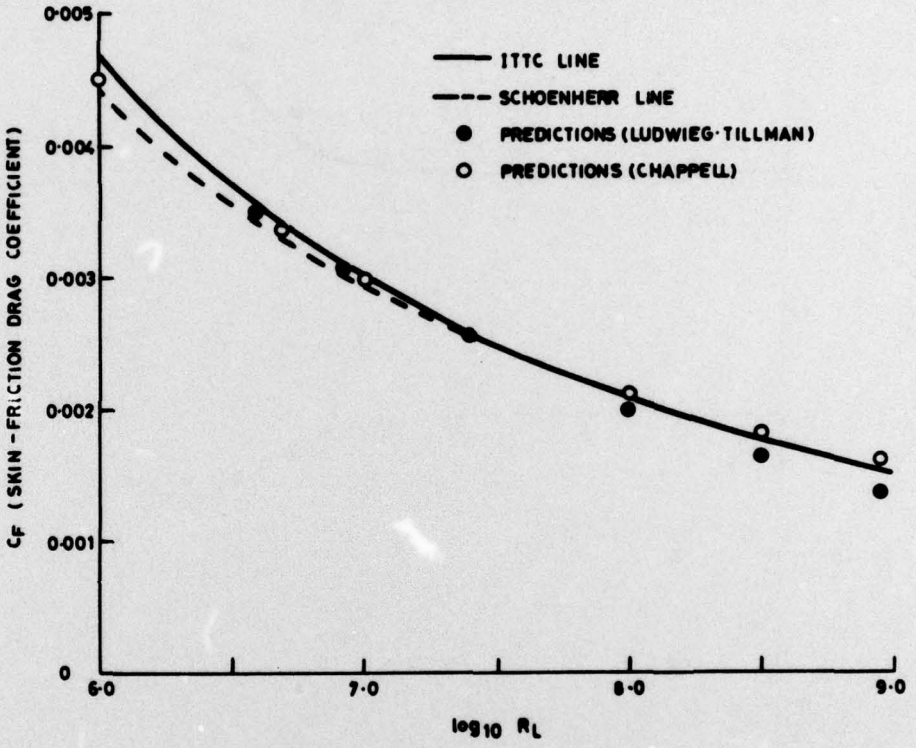

FIG. 6 COMPARISON OF PREDICTIONS USING DIFFERENT SKIN FRICTION LAWS WITH KNOWN CORRELATIONS

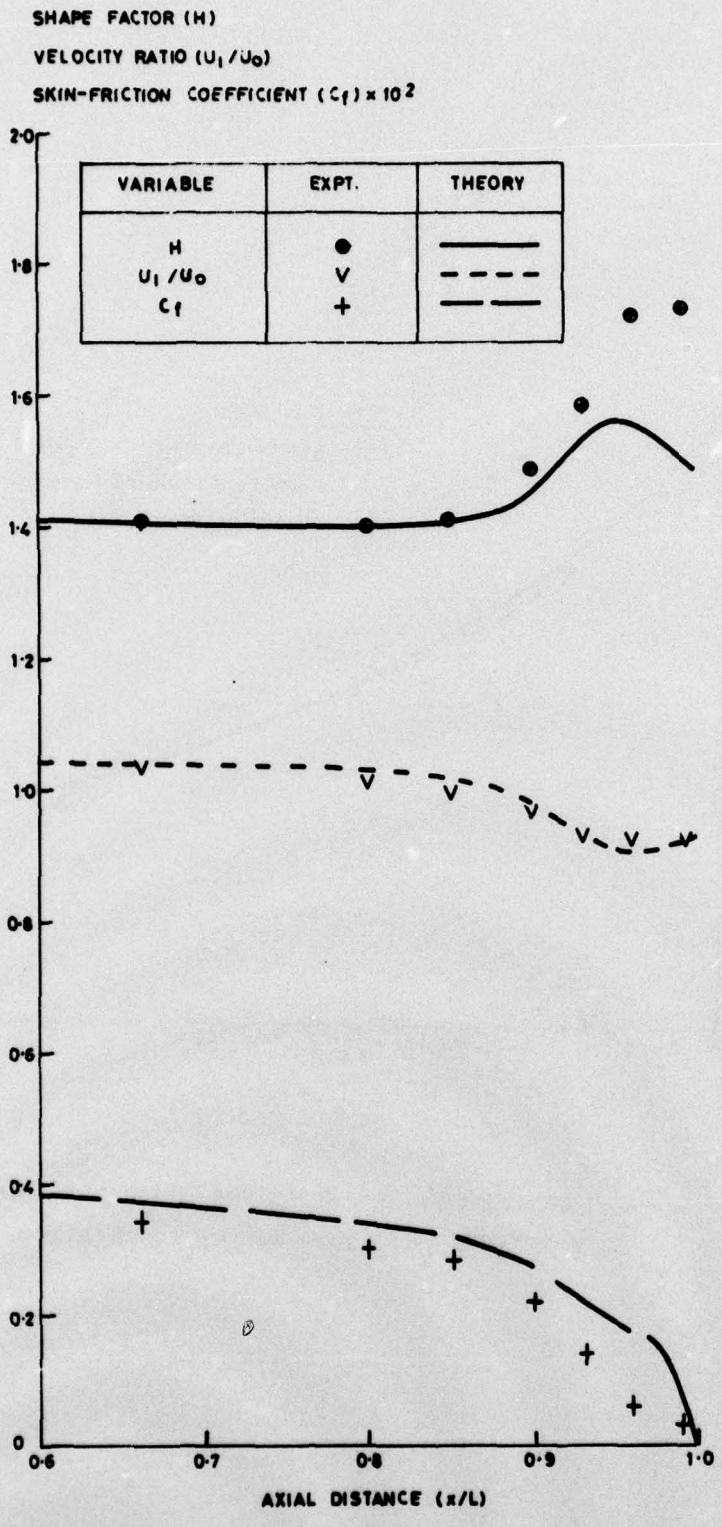

FIG. 7(a) COMPARISON OF PREDICTIONS OF INTEGRAL PARAMETERS WITH THE MEASUREMENTS OF PATEL, ET AL [19] (UNMODIFIED THEORY)

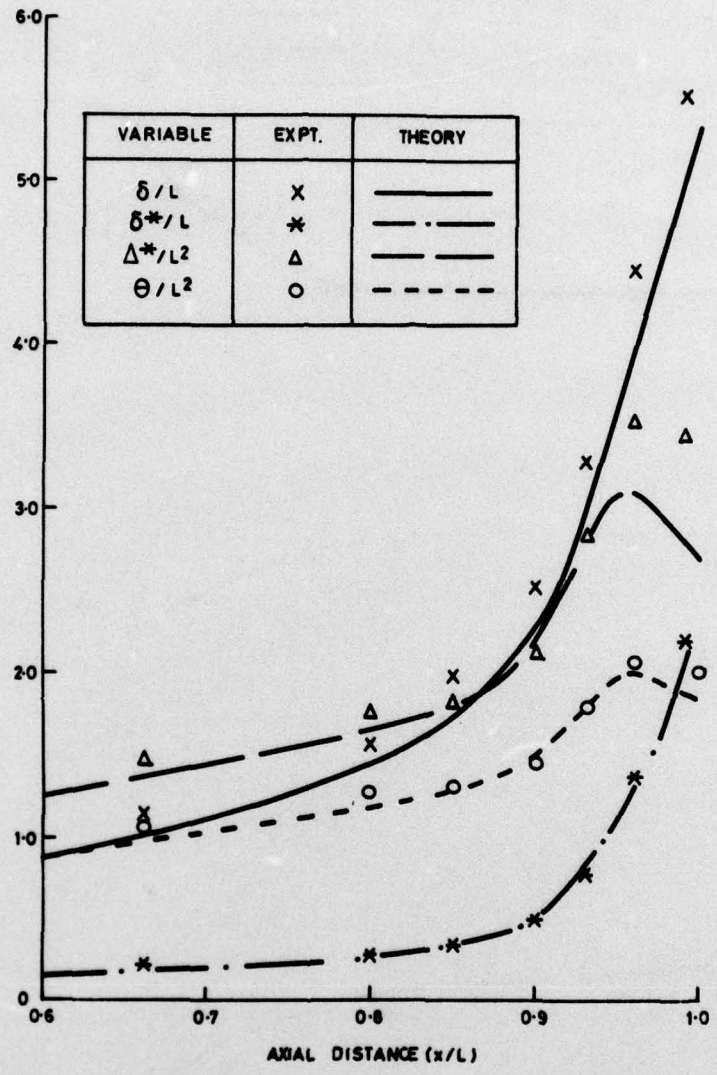

FIG. 7(b) COMPARISON OF PREDICTIONS OF INTEGRAL PARAMETERS WITH THE MEASUREMENTS OF PATEL, ET AL [19] (UNMODIFIED THEORY)

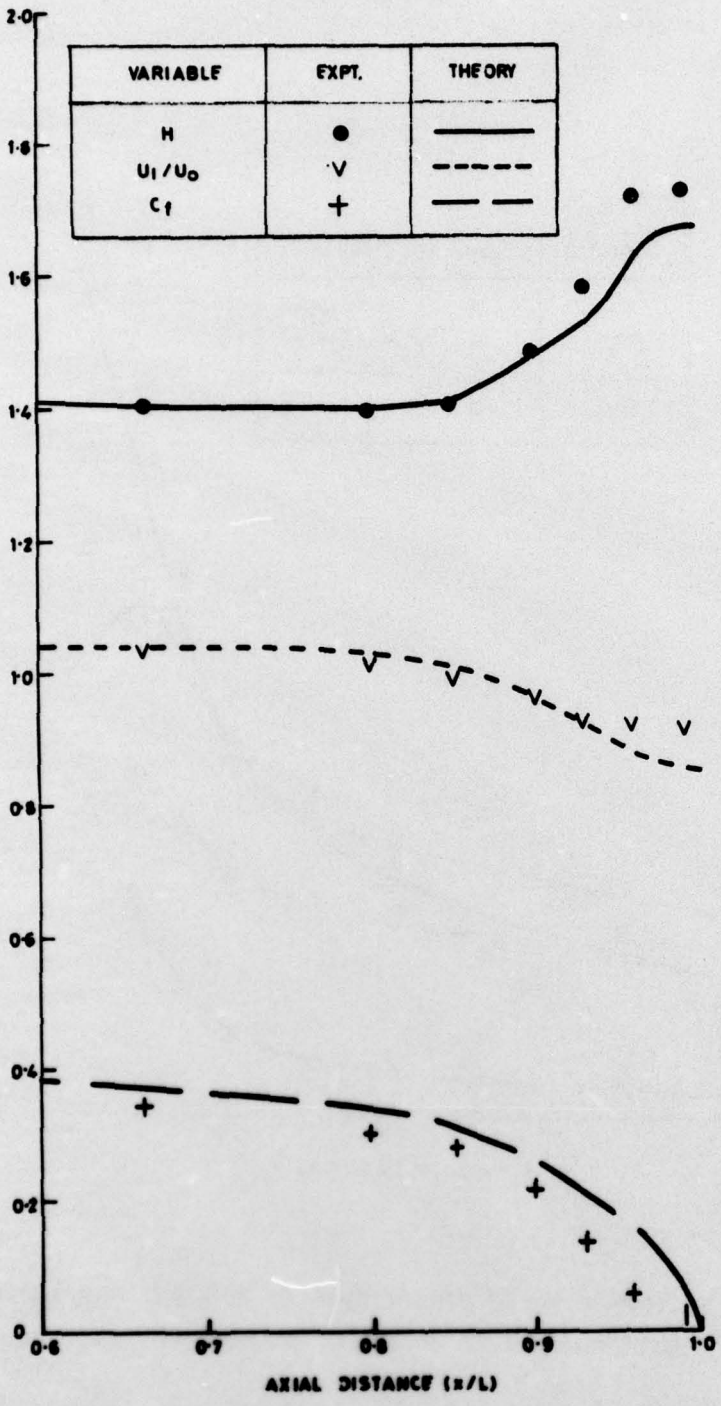

FIG. 8(a) COMPARISON OF PREDICTIONS OF INTEGRAL PARAMETERS WITH THE MEASUREMENTS OF PATEL, ET AL [19] (MODIFIED THEORY)

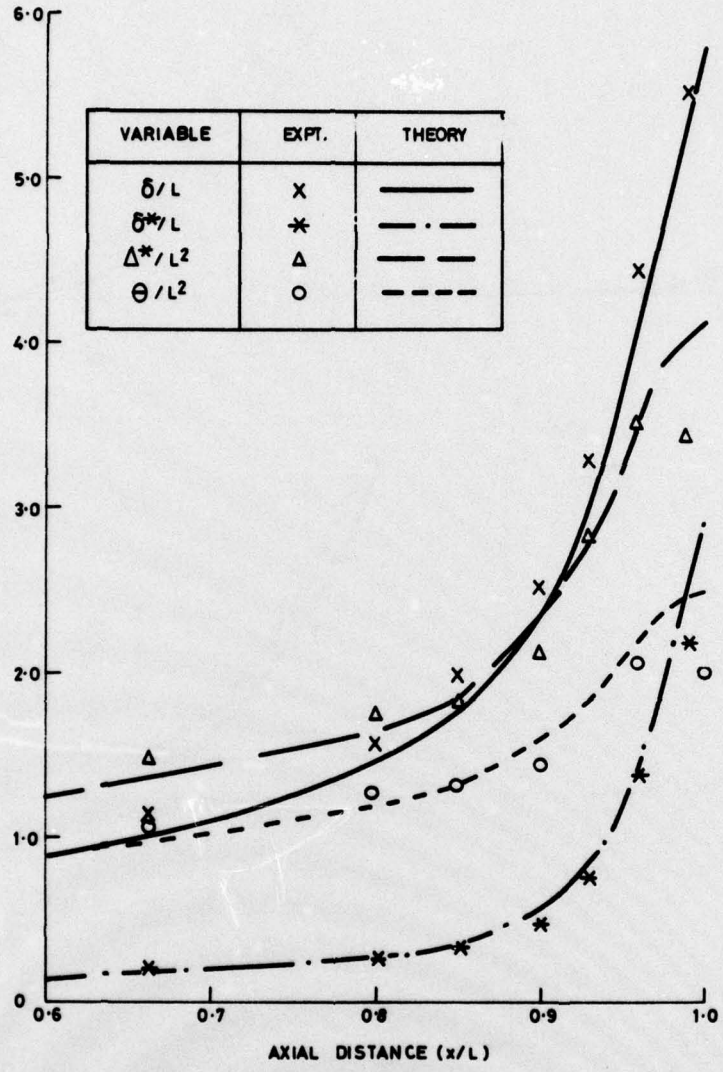

FIG. 8(b) COMPARISON OF PREDICTIONS OF INTEGRAL PARAMETERS WITH THE MEASUREMENTS OF PATEL, ET AL [19] (MODIFIED THEORY)

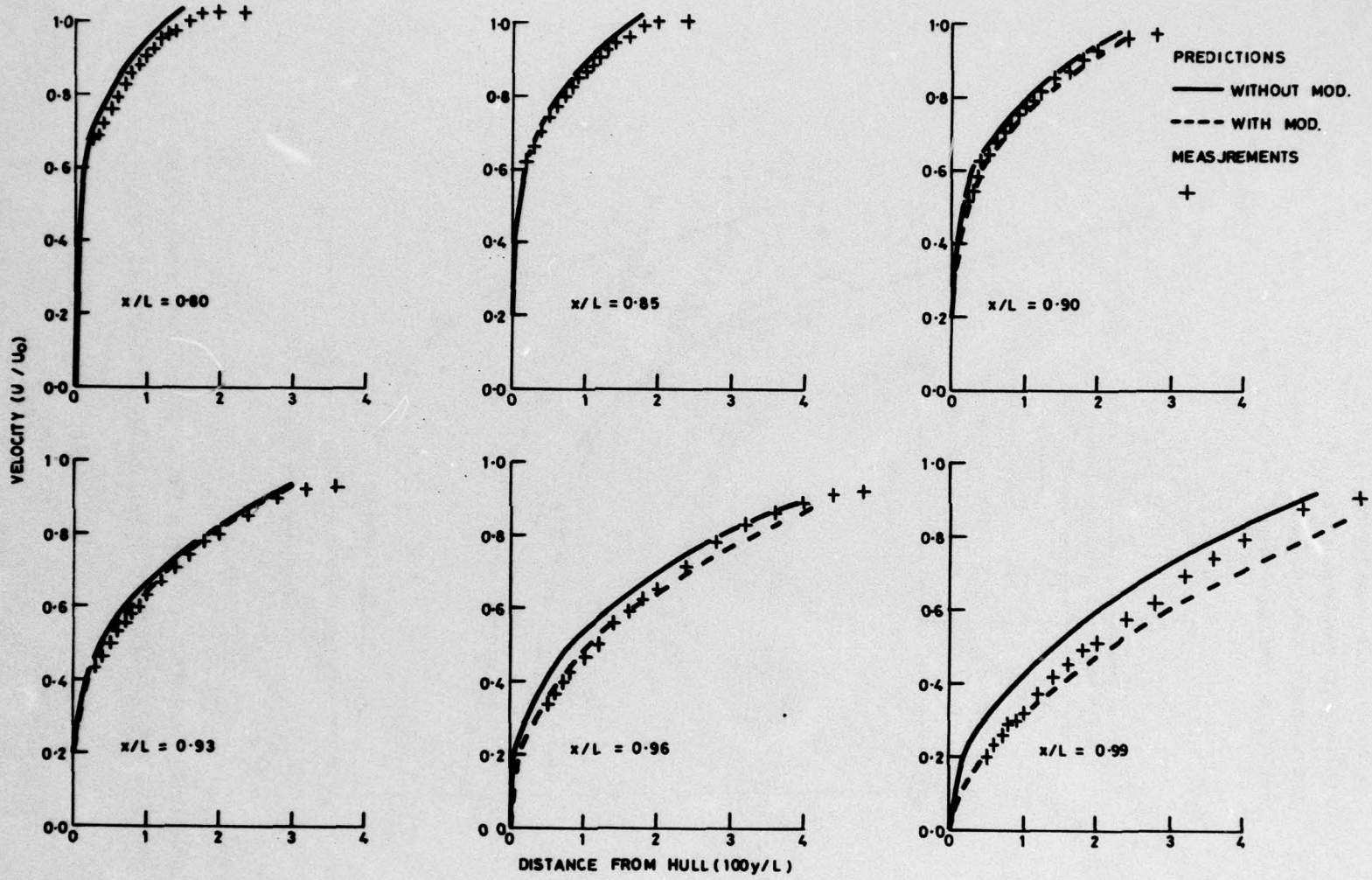

FIG. 9 VELOCITY PREDICTIONS AND MEASUREMENTS ON PATEL ET AL BODY [19]

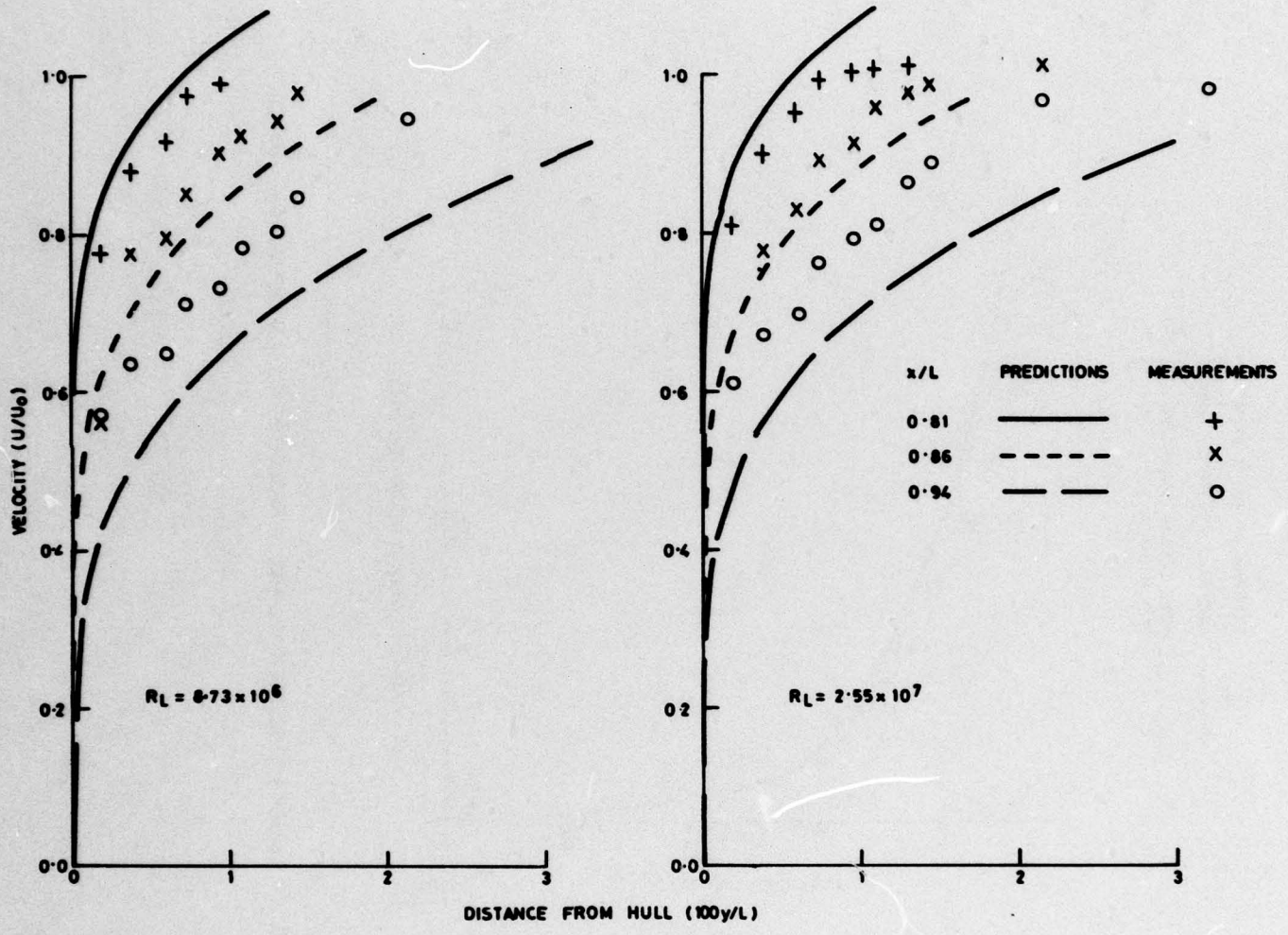

FIG. 10 VELOCITY PREDICTIONS AND MEASUREMENTS ON UNPOWERED TORPEDO MODEL

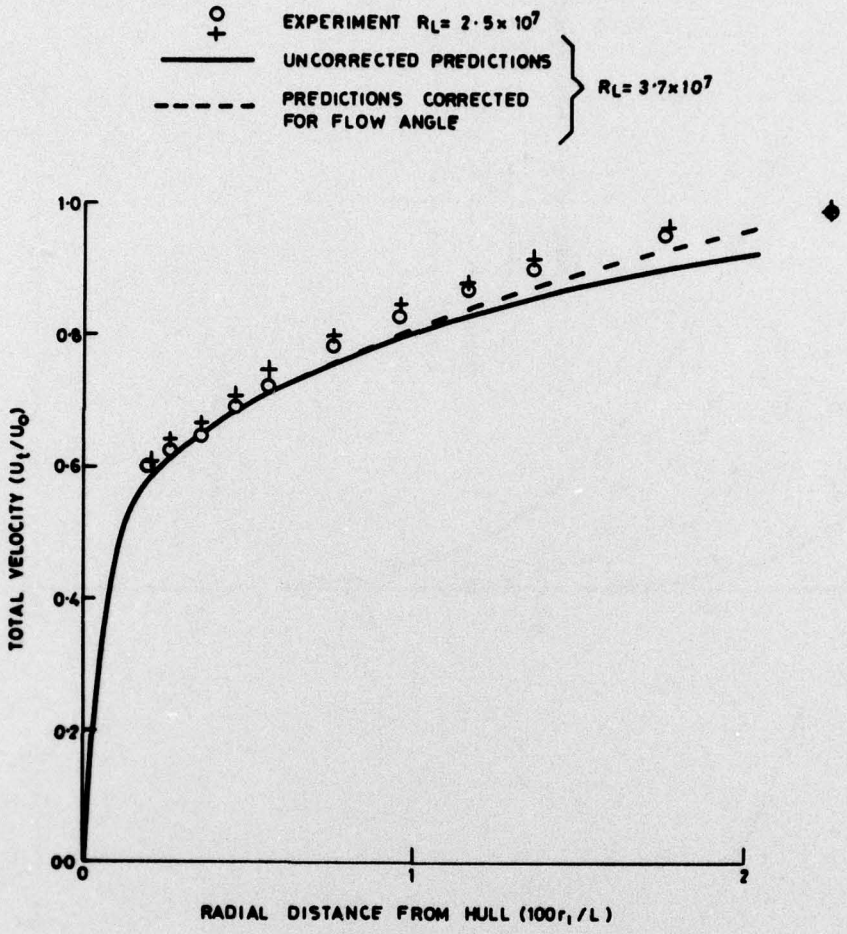

FIG.11 VELOCITY PREDICTIONS AND MEASUREMENTS ON BODY WITH FIN-DUCT

BODY	STREAMLINE BODY	FULL-AFTER-END BODY
MEASUREMENTS	○	△
PREDICTIONS	———	———
BODY SHAPE TO SCALE	- - - - - -	——·——

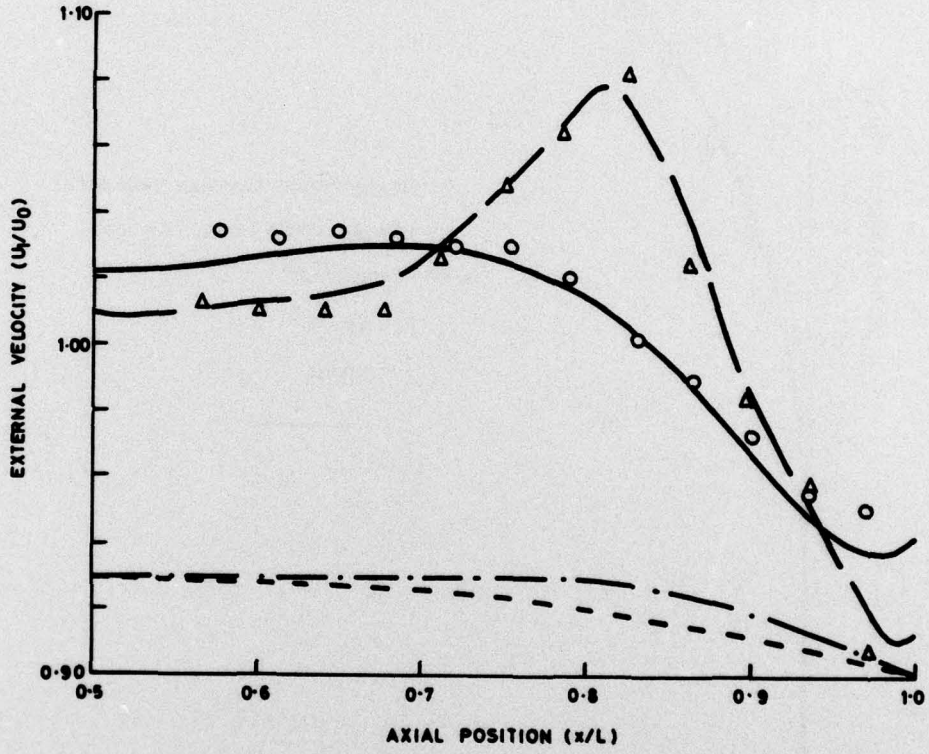

FIG. 12 EXTERNAL VELOCITY PREDICTIONS AND MEASUREMENTS ON TWO BODIES OF REVOLUTION

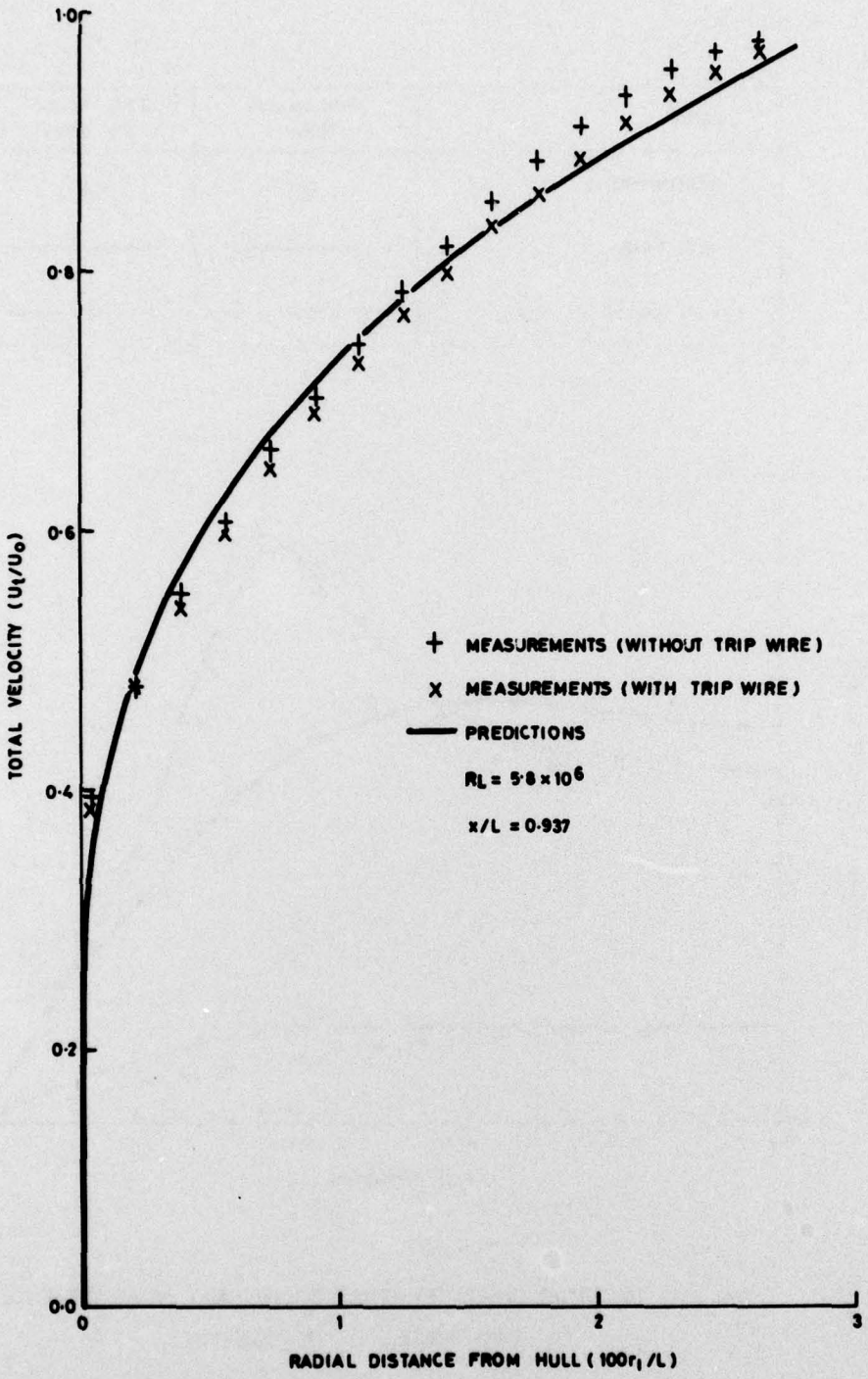

FIG. 13 VELOCITY PREDICTIONS AND MEASUREMENTS ON A STREAMLINE BODY OF REVOLUTION

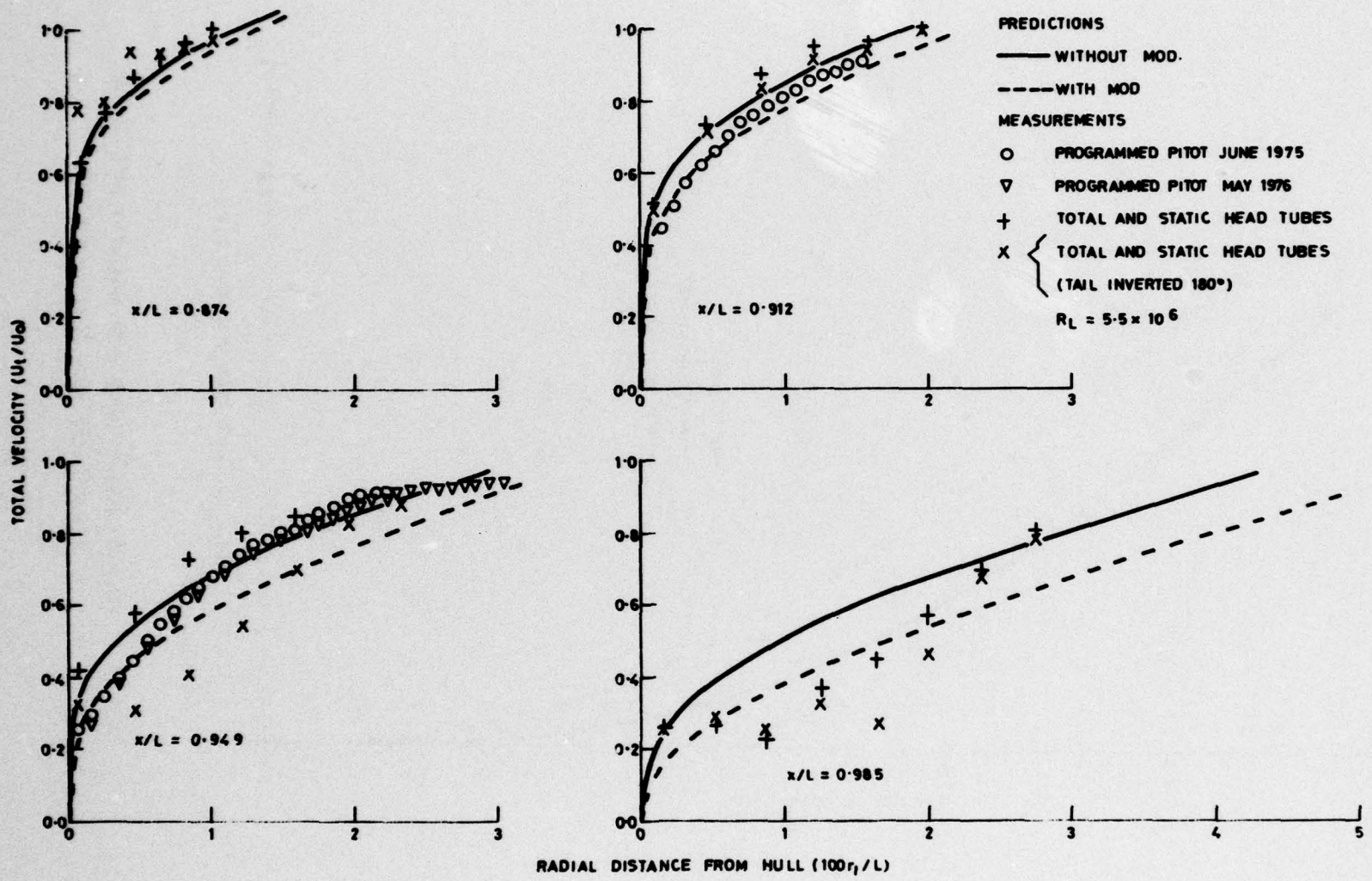

FIG. 14 VELOCITY PREDICTIONS AND MEASUREMENTS ON A BODY OF REVOLUTION WITH FULL AFTER-END

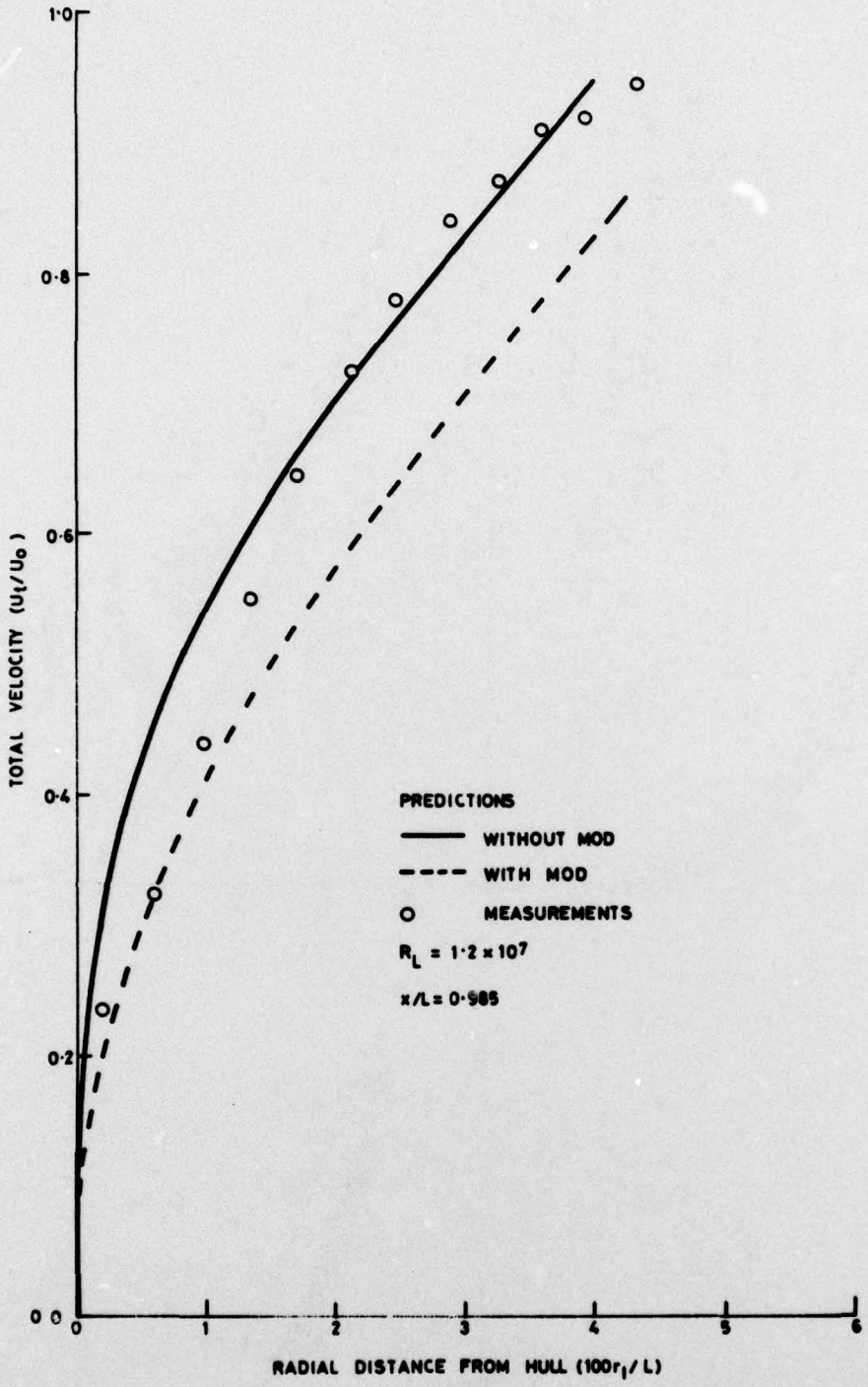

FIG. 15 VELOCITY PREDICTIONS AND MEASUREMENTS ON A BODY OF REVOLUTION WITH FULL AFTER-END

Body	Reference Numbers	Figure Numbers	Length of Nose Section (L_n/D)	Length of Centrebody (L_c/D)	Length of Tail Section (L_t/D)	Length to Diameter Ratio (L/D)	Prismatic Coefficient ($4V/\pi D^2L$)	Reynolds Number ($R_L/10^6$)	Transition Position (x/L)
DTMB4154	26	1(a),4,5	1.600	0.000	2.400	4.000	0.650	Various	0.050
4159	26	1(a),4-6	4.000	0.000	6.000	10.000	0.650	Various	0.050
4165	26,27	1(a),4,5	2.800	0.000	4.200	7.000	0.600	Various	0.050
Torpedo-shaped body	27	1(b),4,5	0.500	4.756	2.744	8.000	0.783	Various	0.029
4620-1	22	2,4,5	0.500	5.840	4.390	10.730	0.802	18.00	0.044
4620-2	22	2,4,5	1.000	5.500	4.390	10.890	0.790	18.00	0.082
4620-3	22	2,4,5	1.820	4.970	4.390	11.180	0.770	18.00	0.150
4620-4	22	2,4,5	3.000	4.170	4.390	11.560	0.744	18.00	0.220
Lyon A	25	3-5	2.000	0.000	3.000	5.000	0.577	2.05	Various
Lyon B	25	3-5	2.000	0.000	3.000	5.000	0.693	2.05	Various
Patel et al	19	7-9	3.000	0.000	3.214	6.214	0.642	1.26	0.048
Unpowered torpedo model	-	10	0.500	5.912	1.977	8.389	0.840	Various	0.029
Body with fin duct	-	11	0.463	5.257	1.934	7.654	0.837	25.00	0.050
Streamline body	-	12,13	3.763	0.388	4.420	8.571	0.696	5.80	0.060
Full after end body	-	12,14,	3.176	3.072	2.186	8.434	0.799	5.50	0.060
		15	3.176	3.336	2.186	8.698	0.807	12.00	0.060

TABLE 1 Details of body shapes and flow conditions.

DISTRIBUTION

	Copy No
DCS(N)/DNOS	1
DGRM	2
DAUWE/DUWP	3
Maritime Gp DRDS(W)	4
OS 9B Navy	5
DG Ships Section 611	6
DGS	7
DGW(N)	8
CS AMTE(H)	9
DRIC	10-32
IEP ABC-17 Standard Distribution	33-38
DTNSRDC Attn: P S Granville	39
ARL/PSU Attn: Dr R E Henderson	40
The Librarian Marconi Space & Defence Systems Ltd Browns Lane, The Airport, Portsmouth PO3 5PH	41
The Deputy Managing Director Engineering Sciences Data Unit Ltd 251-259 Regent Street, London W1R 7AD	42
Dr D F Myring Dept of Mechanical Engineering Salford University, Salford M5 4WT	43
AMTE File	44-60